

Effect of pressure and space between electrodes on the deposition of SiN_xH_y films in a capacitively coupled plasma reactor

Meryem Grari, CifAllah Zoheir, Yasser Yousfi, Abdelhak Benbrik

Citation: Chin. Phys. B, 2021, 30 (**5**): 055205. DOI: 10.1088/1674-1056/abd2a4
Journal homepage: http://cpb.iphy.ac.cn; http://iopscience.iop.org/cpb

What follows is a list of articles you may be interested in

Effect of radio frequency bias on plasma characteristics of inductively coupled argon discharge based on fluid simulations

Xiao-Yan Sun(孙晓艳), Yu-Ru Zhang(张钰如), Sen Chai(柴森), You-Nian Wang(王友年), Yan-Yan Chu(楚艳艳), Jian-Xin He(何建新)
Chin. Phys. B, 2020, 29 (**9**): 095203. DOI: 10.1088/1674-1056/ab9436

Basic features of the multiscale interaction between tearing modes and slab ion-temperature-gradient modes

L Wei(魏来), Z X Wang(王正汹), J Q Li(李继全), Z Q Hu(胡朝清), Y Kishimoto(岸本泰明)
Chin. Phys. B, 2019, 28 (**12**): 125203. DOI: 10.1088/1674-1056/ab5437

Characteristics and underlying physics of ionic wind in dc corona discharge under different polarities

Tongkai Zhang(张桐恺), Yu Zhang(张宇), Qizheng Ji(季启政), Ben Li(李犇), Jiting Ouyang(欧阳吉庭)
Chin. Phys. B, 2019, 28 (**7**): 075202. DOI: 10.1088/1674-1056/28/7/075202

Transmission properties of microwave in rectangular waveguide through argon plasma

Xiaoyu Han(韩晓宇), Dawei Li(李大伟), Meie Chen(陈美娥), Zhan Zhang(张展), Zheng Li(李铮), Yujian Li(李雨键), Junhong Wang(王均宏)
Chin. Phys. B, 2019, 28 (**3**): 035204. DOI: 10.1088/1674-1056/28/3/035204

Effects of secondary electron emission on plasma characteristics in dual-frequency atmospheric pressure helium discharge by fluid modeling

Yi-Nan Wang(王一男), Shuai-Xing Li(李帅星), Yue Liu(刘悦), Li Wang(王莉)
Chin. Phys. B, 2019, 28 (**2**): 025202. DOI: 10.1088/1674-1056/28/2/025202

Effect of pressure and space between electrodes on the deposition of SiN_xH_y films in a capacitively coupled plasma reactor

Meryem Grari[1,†], CifAllah Zoheir[1], Yasser Yousfi[2], and Abdelhak Benbrik[2]

[1] University Mohamed First, Department of Physics, LETSER Laboratory, Oujda, Morocco
[2] University Mohamed First, Department of Mathematics, LANO Laboratory, Oujda, Morocco

(Received 1 October 2020; revised manuscript received 18 November 2020; accepted manuscript online 11 December 2020)

The fluid model, also called the macroscopic model, is commonly used to simulate low temperature and low pressure radiofrequency plasma discharges. By varying the parameters of the model, numerical simulation allows us to study several cases, providing us the physico-chemical information that is often difficult to obtain experimentally. In this work, using the fluid model, we employ numerical simulation to show the effect of pressure and space between the reactor electrodes on the fundamental properties of silicon plasma diluted with ammonia and hydrogen. The results show the evolution of the fundamental characteristics of the plasma discharge as a function of the variation of the pressure and the distance between the electrodes. By examining the pressure-distance product in a range between 0.3 Torr 2.7 cm and 0.7 Torr 4 cm, we have determined the optimal pressure-distance product that allows better deposition of hydrogenated silicon nitride (SiN_xH_y) films which is 0.7 Torr 2.7 cm.

Keywords: fluid model, numerical simulation, SiN_xH_y, capacitively coupled plasma reactor

PACS: 52.65.−y, 52.77.−j, 52.65.Ww, 52.30.−q **DOI:** 10.1088/1674-1056/abd2a4

1. Introduction

The development of semiconductor materials and devices is a powerful driver of many revolutionary changes and innovations in the semiconductor industry. Thin films on silicon (Si) alone have an unsatisfactory performance due to the inherent properties of the material, which motivated researchers to consider introducing a gas mixture. In the literature, the gas mixtures often used are hydrogenated silicon nitride (SiN_xH_y),[1–4] silicon oxide (SiO_x),[5] silicon oxynitride (SiO_xN_y),[6] and amorphous carbon (a-C:H).[7,8]

Hydrogenated silicon nitride (SiN_xH_y) has a band gap of ~ 4.6 eV and a permittivity of ~ 6,[8] making it more suitable for the production of memory elements and charge carrier injectors. Indeed, silicon nitride has a higher density of states at the interface with silicon compared to other gas mixtures. The SiN_xH_y thin film is prepared by the capacitively coupled plasma (CCP) process, comprising the mixture of silane (SiH_4), ammonia (NH_3), and hydrogen (H_2). Other reagents can also be added to this mixture.

Modeling and simulation of plasma discharges are considered as an indispensable tool to improve the knowledge about the physico-chemical processes produced in plasma,[9–11] which helps understand the complex spatio-temporal dynamics of plasma, and also assists in the design of new reactors or the optimization of existing reactors.

The mechanisms of low pressure and low temperature plasma discharges are more complex to study. This complexity is due to the important interactions between particles, which give rise to non-linear phenomena; it is also caused by the presence of very rich chemical kinetics consisting of many reaction processes which are difficult to study quantitatively.

The deposition rate, the uniformity, and the film composition are strongly influenced by the physico-chemical parameters of the reactor, essentially the power, the RF frequency, the pressure, the distance between electrodes, and the gas mixture. Many researchers investigated the effect of varying the physico-chemical parameters of the reactor. For instance, the effect of varying the electrode spacing for $SiH_4/NH_3/N_2$/He mixture was considered in Ref. [3]; the effect of varying the pressure for SiH_4/He mixture was investigated in Ref. [12], many other studies of varying physico-chemical parameters can be found in Refs. [13,14].

In this work, we are interested in the evolution of the fundamental characteristics of hydrogenated silicon nitride RF plasma, in a low pressure and a low temperature CCP reactor, by varying the pressure and space between electrodes. Our objective is to discuss the influence of the latter parameters on the fundamental characteristics of the RF plasma discharge, where the focus is on the pressure-distance product that allows a high deposition rate of the SiN_xH_y thin film and a reduced surface temperature.

2. Plasma discharge

The electrons naturally present in the gas will be accelerated by the external field applied towards the anode, and they collide with the neutral particles and lose energy due to in-

†Corresponding author. E-mail: grarimery@gmail.com

© 2021 Chinese Physical Society and IOP Publishing Ltd

elastic collisions (excitation, dissociation, and ionization of the gas). Each ionizing collision allows the formation of a new electron, which is in his turn accelerated and comes into colliding with the neutral particles (Fig. 1). The repetition of this process allows the number of electrons and positive ions to grow.

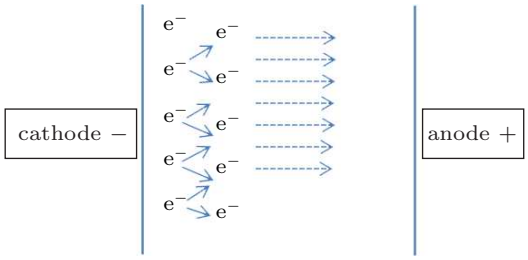


Fig. 1. Secondary electron generation.

The creation of secondary electrons is influenced by the variation of operational parameters, such as frequency and potential,[15–17] the type of gas,[4,5,18] and especially the influence of pressure and reactor geometry.[3,14,19]

2.1. Equations

The general equations of a plasma discharge are resolved to take into account the following hypotheses:

- The gas is weakly ionized.
- The pressure is low.
- No magnetic field is applied.
- The electrons are supposed to have a Maxwellian energy distribution function.
- Mobility and diffusion coefficient satisfy Einstein's relation.

Equations (1)–(7) represent a set of equations solved in a low-temperature plasma simulation.

- Electron and ion transport

$$\frac{\partial n_{\mathrm{i}}}{\partial t}+\nabla \boldsymbol{\Gamma}_{\mathrm{i}}=S_{\mathrm{i}}, \tag{1}$$

$$\frac{\partial n_{\mathrm{e}}}{\partial t}+\nabla \boldsymbol{\Gamma}_{\mathrm{e}}=S_{\mathrm{e}}. \tag{2}$$

- Electron and ion flux

$$\boldsymbol{\Gamma}_{\mathrm{e}}=-n_{\mathrm{e}}\mu_{\mathrm{e}}\boldsymbol{E}-\nabla\left(n_{\mathrm{e}}D_{\mathrm{e}}\right), \tag{3}$$

$$\boldsymbol{\Gamma}_{\mathrm{i}}=n_{\mathrm{i}}\mu_{\mathrm{i}}\boldsymbol{E}-\nabla\left(n_{\mathrm{i}}D_{\mathrm{i}}\right). \tag{4}$$

- Electron energy

$$\frac{\partial n_{\varepsilon}}{\partial t}+\nabla \boldsymbol{\Gamma}_{\varepsilon}+\boldsymbol{E}\boldsymbol{\Gamma}_{\mathrm{e}}=S_{\varepsilon}. \tag{5}$$

- Energy flux

$$\boldsymbol{\Gamma}_{\varepsilon}=-n_{\varepsilon}\mu_{\varepsilon}\boldsymbol{E}-\nabla\left(n_{\varepsilon}D_{\varepsilon}\right). \tag{6}$$

- Electric field

$$\nabla^2\phi=-\frac{e}{\varepsilon_0}\left(n_{\mathrm{i}}-n_{\mathrm{e}}\right). \tag{7}$$

Here e is the elementary charge, n_{e} and n_{i} are respectively the electron and ion densities, $\mu_{\mathrm{e}}=e/(m_{\mathrm{e}}\nu_{\mathrm{eN}})$ and $\mu_{\mathrm{i}}=Z_{\mathrm{i}}e/(m_{\mathrm{i}}\nu_{\mathrm{iN}})$ are respectively the electron and ion mobilities, and $D_{\mathrm{e}}=K_{\mathrm{B}}T_{\mathrm{e}}/(m_{\mathrm{e}}\nu_{\mathrm{eN}})$ and $D_{\mathrm{i}}=K_{\mathrm{B}}T_{\mathrm{i}}/(m_{\mathrm{i}}\nu_{\mathrm{iN}})$ are respectively the electron and ion diffusivity, m_e is the electron masse, ν_{eN} and ν_{iN} are the electron and ion-neutral collision frequencies, $n_{\varepsilon}=n_{\mathrm{e}}\varepsilon$ and $D_{\varepsilon}=n_{\mathrm{e}}D_{\mathrm{e}}$ are the electron energy density and electron energy diffusivity where ε is the electron energy, $\boldsymbol{E}=-\nabla\phi$ is the electric field where ϕ is the electrical potential, T_{e} and T_{i} are respectively the electronic and ionic temperatures.

- Source terms

$$S_{\mathrm{e}}=\sum x_r k_r N_{\mathrm{n}} n_{\mathrm{e}}, \tag{8}$$

$$S_{\mathrm{i}}=\sum x_r k_r N_{\mathrm{n}} n_{\mathrm{e}}, \tag{9}$$

$$S_{\varepsilon}=\sum x_r k_r N_{\mathrm{n}} n_{\mathrm{e}} \varepsilon_r, \tag{10}$$

$$k_r=\gamma\int \varepsilon\sigma_r(\varepsilon)f(\varepsilon)\,\mathrm{d}\varepsilon, \tag{11}$$

where x_r is the molar fraction of species r, N_{n} is the total density of the neutrals, k_r is the kinetic coefficient, $\sigma_r(\varepsilon)$ are the cross sections of elastic and inelastic collisions, $f(\varepsilon)$ is the Maxwellian electronic energy distribution function.

2.2. Chemical reactions

Our model considers elastic and inelastic excitation and ionization collisions. From the radicals formed, a multitude of reactions can take place within the plasma giving compounds that will intervene in the deposition. The calculation of the source term (Eqs. (8)–(10)) is crucial for the selection of effective sections of the different reactions taken into account.[1,2,16] Thus, a wide range of energy was considered for the most reactive collisions.

The predominant reactions occurring in plasma are shown in Tables 1 and 2.

Table 1. Energy of reactions NH_3 and SiH_4.

Reaction	Energy (eV)
1: $e+NH_3 \Longrightarrow e+NH_3^*$	0.42
2: $e+NH_3 \Longrightarrow 2e+NH_3^+$	10.2
3: $e+SiH_4 \Longrightarrow e+SiH_4^*$	0.27
4: $e+SiH_4 \Longrightarrow e+SiH_3+H$	4
5: $e+SiH_4 \Longrightarrow e+SiH_2+H$	2.2

The cross sections data used in simulation, SiH_4, NH_3, and H_2 collisions are given by Hayashi.[20]

Table 2. Kinetic coefficient of reactions NH_3, SiH_4, and H_2.

Reactions	Kinetic coefficient [m^3/(s·mol)]
6 : $SiH_4 + SiH_2 \Longrightarrow Si_2H_6$	2.8×10^7
7 : $SiH_4 + H \Longrightarrow SiH_3 + H_2$	1.9×10^6
8 : $SiH_4 + NH \Longrightarrow HSiNH_2 + H_2$	3.6×10^7
9 : $SiH_4 + NH_2 \Longrightarrow SiH_3 + NH_3$	2.4×10^6
10 : $SiH_4 + NH \Longrightarrow SiH_3 + NH_2$	2.4×10^7
11: $H_2^+ + H_2 \Longrightarrow H_3^+ + H$	1.26×10^9
12: $SiH_4 + H_3^+ \Longrightarrow SiH_3^+ + H_2 + H_2$	3.1×10^8
13: $SiH_4 + H_2^+ \Longrightarrow SiH_2^+ + H_2 + H_2$	3.96×10^7
14: $SiH_4 + H_2^+ \Longrightarrow SiH_3^+ + H_2 + H$	3.75×10^8
15: $SiH_3^+ + SiH_4 \Longrightarrow Si_2H_2^+ + H_2 + H_2 + H$	15.05×10^6
16: $SiH_4 + H \Longrightarrow H_2 + SiH_3$	2.6×10^5
17: $SiH_4 + SiH_3 \Longrightarrow Si_2H_5 + H_2$	1.07×10^3
18: $SiH_3 + SiH_3 \Longrightarrow SiH_2 + SiH_4$	9.03×10^7
19: $SiH_4 + H \Longrightarrow SiH_2 + H$	6.02×10^7
20: $SiH_4 + SiH_2 \Longrightarrow Si_2H_5$	2.26×10^5
21: $SiH_4 + Si_2H_5 \Longrightarrow Si_3H_8$	6.02×10^6
22: $SiH_2 + H \Longrightarrow SiH + H_2$	4.79×10^5
23: $SiH_2 + H \Longrightarrow SiH_3$	6.68×10^5
24: $NH_2 + NH_2 \Longrightarrow N_2H_4$	6×10^5
25: $SiH + H_2 \Longrightarrow SiH_3$	11.9×10^5
26: $NH_2 + H \Longrightarrow NH_3$	6×10^4
27: $SiH_4 + NH_2 \Longrightarrow SiH_3 + NH_3$	2.4×10^7

2.3. Boundary conditions

The boundary conditions used in this section are similar to those presented in Refs. [1,2,14].

The limit condition for the Poisson equation is the amount of potential on the electrodes: $V = 0$ electrical potential at the cathode. $V_{rf} = V_0 \sin(\omega t)$ electrical potential at the anode. Here, ω and V_{rf} are respectively the pulsation and the amplitude of the alternative voltages.

The limit condition of electrons has a proportional flux to their thermal velocity, whereas ions have a zero gradient near the walls

$$\Gamma_e = 5\frac{v_{th} n_e}{4} - \gamma_p \Gamma_i, \tag{12}$$

$$\Gamma_i = -\mu_i n_i \nabla V, \tag{13}$$

where v_{th} is the thermal velocity of electrons, and γ_p is the secondary electron emission coefficient that is initiated by the collision of ions with the surface.

Quantities v_{th} and q_e are calculated by

$$q_e = \frac{v_{th} k_B}{4}, \tag{14}$$

$$v_{th} = \sqrt{\frac{8 k_B T_e}{\pi m_e}}. \tag{15}$$

3. Results and discussion

The CCP reactor is driven by a sinusoidal voltage with a frequency of 13.56 MHz at a temperature of 500 K. A silane mixture diluted with hydrogen and ammonia is used as a deposition precursor in this simulation. The RF voltage taken is 130 V, applied to the anode at pressure p and inter-electrode distance d. The results are presented at a final computation time of the order of 7.37 μs.

Figures 2–5 show the variation of electron density, temperature, electric field, and electron velocity as a function of pressure, taking a pressure margin between 0.3 and 1.2 Torr for an inter-electrode distance of 2.7 cm. Keeping the pressure at 0.3 Torr and varying the distance between 2.7 and 7 cm, Figures 6–10 respectively show the variation of electron density, temperature, electric field, and velocity as a function of the distance between the electrodes. Finally, figures 11 and 12 show the electron density and temperature for a pressure-distance product noted $p \times d$.

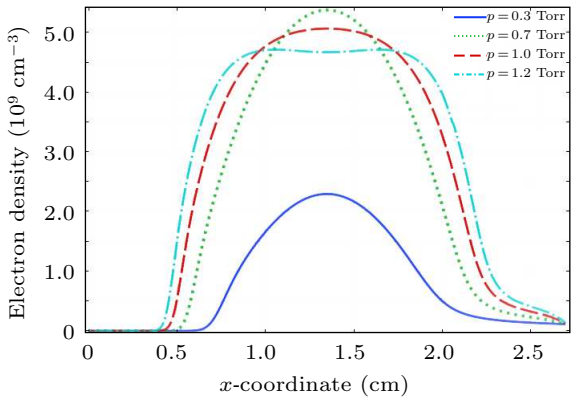


Fig. 2. Variation of electron density (cm^{-3}) as a function of pressure.

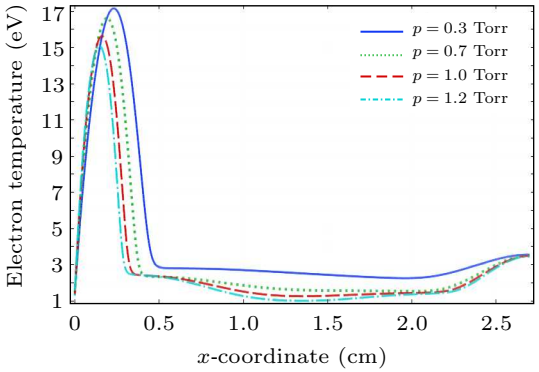


Fig. 3. Electronic temperature variation (eV) as a function of pressure.

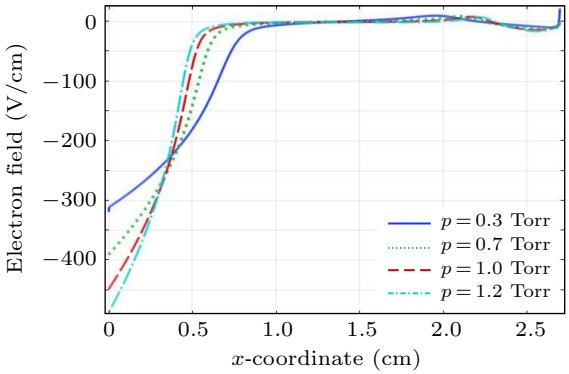


Fig. 4. Electric field variation (V/cm) as a function of pressure.

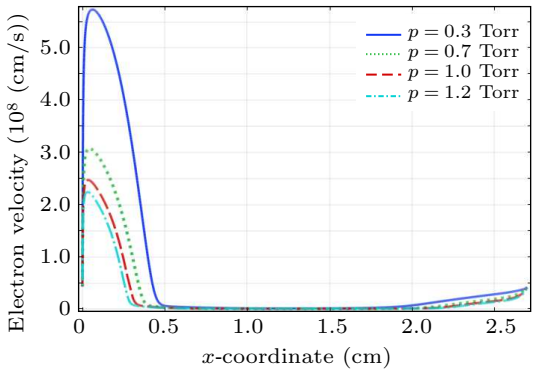


Fig. 5. Electronic velocity variation (cm/s) as a function of pressure.

By increasing the pressure in the deposition system up to 0.7 Torr, the radical density rises as the precursor density grows (Fig. 2). Another effect of increasing the pressure in the deposition chamber is that it leads to the accumulation of radicals in the region between sheaths, which reduces the temperature in this region (Fig. 3). According to Bavafa,[14] the typical pressure in a capacitively coupled PECVD process mostly varies between 0.05 and 1 Torr. Therefore, when we exceed the limits of the physical parameters (0.05 and 1 Torr), we should expect anomalies. Indeed, the simulation results (Fig. 2) show that the electron density becomes less important and almost bipolar once the pressure reaches 1.2 Torr, which does not present the characteristics of RF plasma discharge.

An electric field is introduced and added to the field created by the charges in the plasma. Figure 4 shows that it becomes large (in absolute value) when the pressure increases, causing a large displacement of electrons and ions. In the cathode region, the electrons are strongly accelerated, which explains the high speed (Fig. 5) as well as the high temperature in this region (Fig. 3). As we get closer to the anode region, we notice that there is an inversion of the field; as a consequence, the electrons gain energy which accelerates the electrons towards the electrode (Fig. 5).

The influence of the distance between electrodes on the discharge is shown in Figs. 6–10. For a small distance between 2.7 and 4 cm, the electron density increases even as the distance increases (Fig. 6). This means that this range gives the electrons enough space for the creation of secondary electrons, which leads to a large migration of electrons to the cathode, which explains the high temperature shown in Fig. 8. When the distance becomes larger (between 5 and 7 cm, Fig. 7), the collisions between electrons will be small, and consequently the creation of secondary electrons will be low. Also, when the distance increases, the plasma density region moves closer to the anode (Figs. 6 and 7). Figure 9 shows that the electric field decreases (in absolute values) as the distance between electrodes increases, which explains the decrease in electron velocity (Fig. 10).

The evolution of these characteristics corresponds well to the theory of an RF plasma discharge given the density and energy equations.[21,22] Indeed, these results are in accordance with the electron temperature and electric field distributions shown in the literature.[14,19,23]

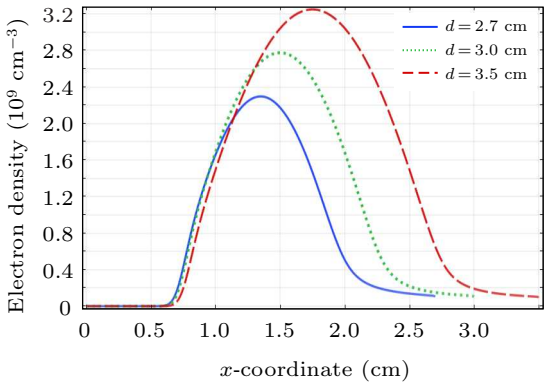


Fig. 6. Electron density variation (cm^{-3}) as a function of the distance between 2.7 and 3.5 cm.

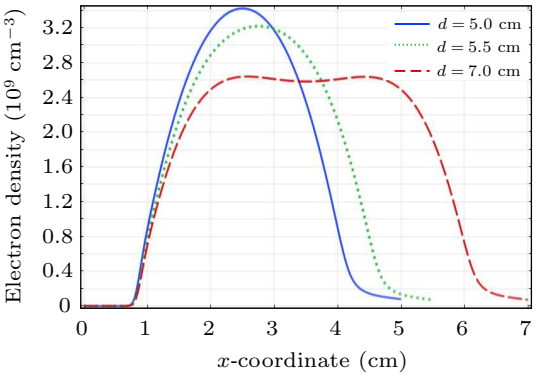


Fig. 7. Electron density variation (cm^{-3}) as a function of the distance between 5 and 7 cm.

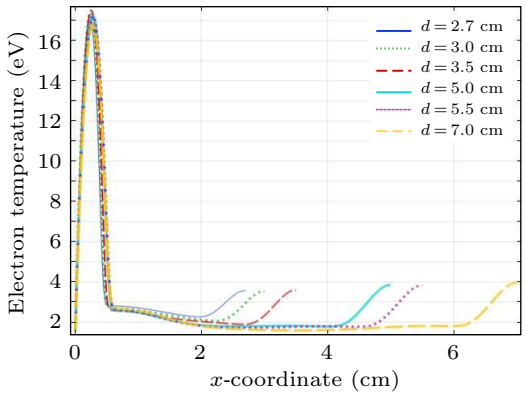


Fig. 8. Electronic temperature variation (eV) as a function of distance.

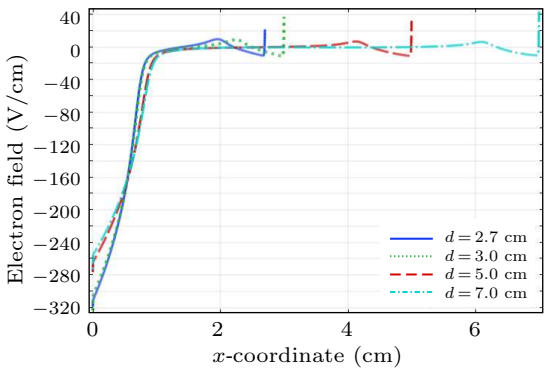


Fig. 9. Electric field variation (V/cm) as a function of distance.

In order to determine an optimal pressure-electrode distance $p \times d$ product, we will vary both the pressure (between 0.3 and 0.7 Torr) and the inter-electrode distance (between 2.7 and 4 cm) at the same time. The optimal $p \times d$ choice is the best compromise between a high electron density and a low surface temperature. Figures 11 and 12 show the variation in electron density and temperature for different pressure-distance $p \times d$ products.

Figure 11 shows that the product 0.7 Torr 2.7 cm surpasses all other electronic densities; it has the highest estimated density of about 5.5×10^9 cm^{-3}, followed by the product 0.5 Torr 3cm with a density close to 4.7×10^9 cm^{-3} and the product 0.5 Torr 4cm with a density close to 4.2×10^9 cm^{-3}. The product 0.7 Torr 4 cm shows an electron density less important with a bipolar shape, which is inadequate in our context. Finally, the lowest of the products is the 0.3 Torr 2.7 cm, which barely reaches 2.3×10^9 cm^{-3}. By examining Fig. 12, we find that the products have almost the same anode temperature with a value close to 3.5 eV. Based on the two criteria of electron density and surface temperature, we can deduce that the product 0.7 Torr 2.7 cm is the optimal choice with respect to all products considered in this simulation. Therefore, this product will allow a better deposition rate, which improves the uniformity of the hydrogenated silicon nitride thin film.

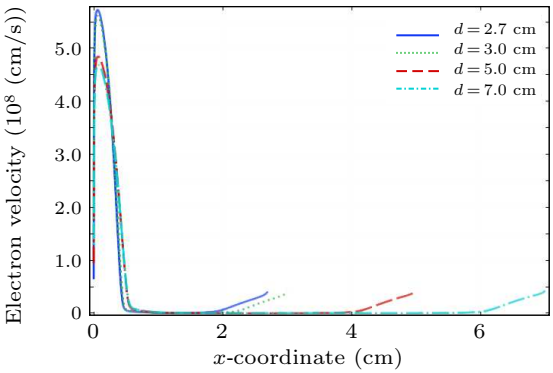


Fig. 10. Electronic velocity variation (cm/s) as a function of distance.

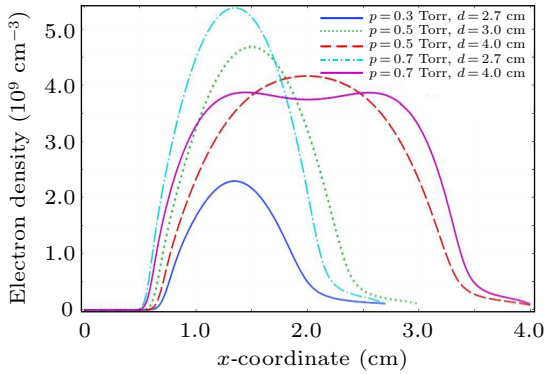


Fig. 11. Electronic density distribution in cm^{-3} for the product $p\times d$.

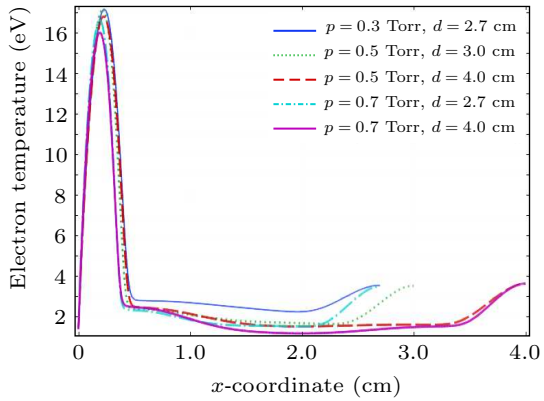


Fig. 12. Electronic temperature distribution in eV for the product $p \times d$.

4. Conclusion and perspectives

Understanding the RF discharges used in the processing of electronic materials requires a valuable study of the various parameters of discharge reactors. In our work, we were interested in modeling a thin film deposit in a CCP reactor driven by a sinusoidal voltage of 130 V and a frequency of 13.56 MHz at a temperature of 500 K. We used a silane mixture diluted with hydrogen and ammonia for a variable electrode distance d and pressure p. The fluid model used is solved using the one-dimensional finite element method.

The results of the numerical simulation that we performed by varying the pressure and the distance between electrodes have revealed the importance of these factors in the variation of the fundamental characteristics of the discharge and consequently influencing the quality of the deposit in the reactor. Moreover, by considering the criteria of electron density and surface temperature and examining a wide range of products, we were able to select an optimal pressure-distance product that is 0.7 Torr 2.7 cm. The use of this product will result in the creation of a more reactive plasma volume, which allows an increase in deposition speed and a more conformal surface treatment. Consequently, enhance the quality of the deposit in the CCP reactor.

References

[1] Grari M and Zoheir C 2020 *Int. J. Eng.* **33** 1449
[2] Grari M and Zoheir C 2021 *Proceedings of the 2nd International Conference on Electronic Engineering and Renewable Energy,* ICEERE 2020, Springer, Singapore, p. 230
[3] Kim H J, Yang W and Joo J 2015 *J. Appl. Phys.* **118** 043304
[4] Kim H J and Lee H J 2016 *Plasma Sources Sci. Technol.* **25** 035006
[5] Bonilla R S, Reichel C, Hermle M and Wilshaw P R 2014 *J. Appl. Phys.* **115** 144105
[6] Gritsenko V A 2009 *Physics-Uspekhi* **52** 869
[7] Ferre R, Martín I, Ortega P, Vetter M, Torres I and Alcubilla R 2006 *J. Appl. Phys.* **100** 073703
[8] Van Laar J H, Bissett H, Barry J C, Van der Walt I J and Crouse P L 2018 *J. Eur. Ceram. Soc.* **38** 1197
[9] Qian M Y, Yang C Y, Chen X C, Ni G S, Liu S and Wang D Z 2015 *Chin. Phys. Lett.* **32** 075202
[10] Yu M H 2019 *Acta. Phys. Sin.* **68** 185202 (in Chinese)
[11] Liu C Y, Wu B, Qian J P, Li G Q, Hou Y W, Wei W, Chen M X, Lei M Z and Guo Y 2020 *Chin. Phys. B* **29** 025202
[12] Kim H J and Lee H J 2017 *Plasma Sources Sci. Technol.* **26** 085003
[13] Kim H C, Iza F, Yang S S, Radmilović-Radjenović M and Lee J K 2005 *J. Phys. D: Appl. Phys.* **38** R283
[14] Bavafa M, Ilati H and Rashidian B 2008 *Semicond. Sci. Tech.* **23** 095023

[15] Lymberopoulos D P and Economou D J 1995 *J. Res. Natl. Inst. Stan.* **100** 473
[16] Hao D X, Chen J, Ji L H and Sun Y C 2012 *J. Semicond.* **33** 104004
[17] Rebiai S, Bahouh H and Sahli S 2013 *IEEE Trans. Dielectr. Electr. Insul.* **20** 1616
[18] Grari M and Zoheir C 2019 *Materials Today: Proceedings.* **13** 888
[19] Boeuf J P and Pitchford L C 1995 *Phys. Rev. E* **51** 1376
[20] Hayashi database 2016 www.lxcat.net, retrieved on October 27, 2016
[21] Kim H J and Lee H J 2017 *Plasma Sources Sci. Technol.* **26** 085003
[22] Lieberman M A and Lichtenberg A J 2005 *Principles of plasma discharges and materials processing* (John Wiley & Sons) p. 387
[23] Samir T, Liu Y, Zhao L L and Zhou Y W 2017 *Chin. Phys. B* **26** 115201